Low-temperature incommensurate-commensurate phase sequence of $(C_3H_7ND_3)_2MnCl_4$

P. Muralt* and R. Kind
Laboratorium für Festkörperphysik, Eidgenössische Technische Hochschule Zürich–Hönggerberg, CH-8093 Zürich, Switzerland

W. Bührer
Eidgenössisches Institut für Reaktorforschung, CH-5503 Würenlingen, Switzerland

(Received 8 September 1987)

The perovskite-type layer-structure compound $(C_3H_7ND_3)_2MnCl_4$ [bis-(propylammonium)manganese tetrachloride (PAMC)] exhibits an extraordinary rich structural phase sequence with six different phases ($\alpha,\beta,\gamma,\delta,\epsilon,\zeta$), two of which ($\gamma$ and ϵ) are incommensurately modulated. In this contribution we focus on the δ-ϵ-ζ sequence which shows a peculiar switching of the modulation wave vector from $(\frac{1}{3}+\delta)\mathbf{a}^*$ to $(\mathbf{a}^*\pm\mathbf{b}^*)/3$. The study was performed by means of ^{35}Cl nuclear quadrupole resonance (NQR) and deuteron and proton NMR, as well as elastic neutron scattering. It was possible to determine the rotational components of the polarization vector for the N—C bond. A microscopic model is proposed which takes couplings between lattice waves and fluctuations of the rotational disorder of the propyl-ammonium (PA) chains into account. The origin of the incommensurate modulation of the ϵ phase is the competition between the ND_3 ordering in the Cl-octahedra cavities and the PA-chain packing due to van der Waals interactions. Because of intralayer short-range interactions via the hydrogen bonds the ND_3 ordering is incompatible with a continuous incommensurate modulation. This leads to an additional symmetry breaking of the translational symmetry, which was observed in the ^{35}Cl-NQR spectra. The complete ordering of the ND_3 groups reduces the PA dynamics in such a way that the interlayer interaction through the PA chains changes sign, which leads to the switching of the wave vector.

I. INTRODUCTION

The perovskite-type layer compound $(C_3H_7NH_3)_2MnCl_4$ [bis-(propylammonium)manganese tetrachloride (PAMC)] exhibits an unusual structural phase sequence with two incommensurate phases. The high-temperature incommensurate phase (γ phase) is the only one known where the amplitude of the modulation wave vanishes and the high-symmetry phase reenters on lowering the temperature.[1,2] The low-temperature incommensurate phase (ϵ phase) has a peculiar lock-in transition where the wave vector $(\frac{1}{3}+\delta)\mathbf{a}^*$ of the incommensurate modulation switches to a commensurate value of $\frac{1}{3}(\mathbf{a}^*\pm\mathbf{b}^*)$,[3] i.e., instead of a triplication along the a axis, a triplication along one of the two basis vectors $\mathbf{t}_1$ or $\mathbf{t}_2$ of the primitive unit cell occurs. Such a behavior is rather exceptional. A similar switching has so far been observed only in crystals of biphenyl, where the modulation wave vector switches between two incommensurate positions.[4] In this article new results of the low-temperature δ-ϵ-ζ sequence are presented.

The high-symmetry δ phase has space group $Cmca$ with $Z=2$.[5,6] The phase transition to the incommensurate ϵ phase occurs at $T_I=162.5$ K. The wave vector locks in at $T_c=114.5$ K. Both transition temperatures given here are for the partially deuterated compound (see below).

The two phase transitions were discovered by Depmeier, Felsche, and Wildermut[7] with the help of differential scanning calorimetry and x-ray scattering. Elastic neutron scattering experiments performed by Depmeier and Mason some years later revealed the incommensurability of the ϵ phase[8] and the switching of direction of the wave vector at the ϵ-ζ transition.[3] The superspace group $P\frac{Cmca}{11s}$ for ϵ PAMC was deduced from x-ray scattering[9] and elastic neutron scattering.[8] According to the same authors the symmetry of ζ PAMC belongs to the Bravais class $P2/m$, but has not yet been determined in detail by means of scattering experiments.[3] Group-theoretical arguments in combination with our nuclear quadrupole resonance (NQR) results allow, however, to determine the space group unambiguously. The space group $P112_1/n$ is derived, as will be shown later.

PAMC belongs to the family of perovskite-type layer compounds of the general formula $(C_nH_{2n+1}NH_3)_2MCl_4$ (where $M=$Mn, Cu, Cd, Fe). The schematic structure of this family is shown in Fig. 1(a). The layers consist of corner sharing $(MnCl_6)^2$ octahedra yielding a chessboard-like pattern. They are sandwiched between rigid but dynamically disordered $(C_nH_{2n+1}NH_3)^+$ chains. These are attached to the layers via hydrogen bonds between the NH_3 heads and the chlorine ions: one bridge to an in-plane chlorine site [Cl(1)] and two bridges to out-of-plane chlorine sites [Cl(2)].[10] The NH_3 heads occupy the essentially quadratic cavities between neighboring octahedra.

The compounds with short hydrocarbon chains ($n<3$) are known to exhibit several structural phase transitions which are connected with reorientational jumps of the chains between four orientations,[11,12] according to the

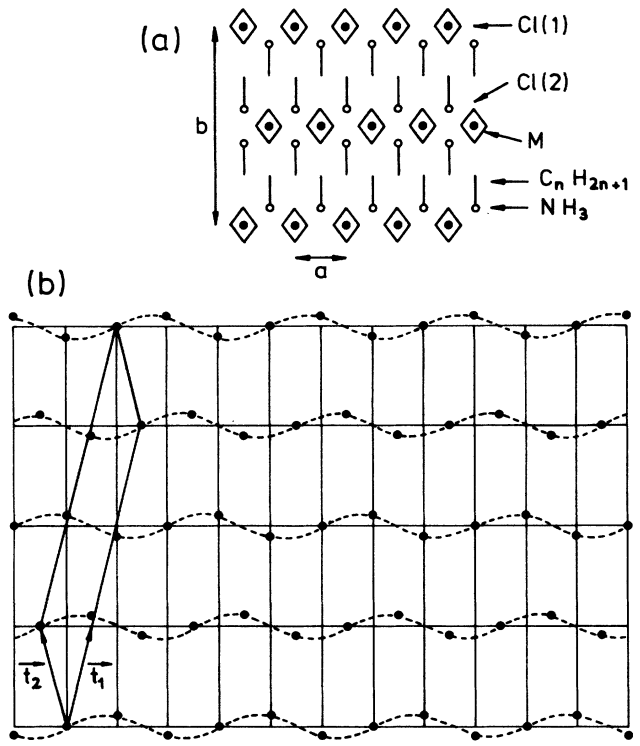

FIG. 1. (a) Schematic structure of the perovskite-type layer compounds of the formula $(C_nH_{2n+1}NH_3)_2MCl_4$ (M=Mn, Cu, Fe, Cd). The metal sites are connected via chlorine ions along the ⟨101⟩ directions of the room-temperature phase (*Cmca*). (b) Schematic view of the structure of ζ PAMC. The drawing shows in an exaggerated manner a transverse wave running along $\mathbf{t}_1$ giving a triplication of the unit cell along $\mathbf{t}_1$. The dots indicate manganese sites in the (001) plane.

four possible ways the NH_3 heads can couple to the layer. These kind of phase transitions can be observed by means of quadrupole perturbed deuteron NMR of the partially deuterated crystal.[13] It is sufficient to exchange the ammonium protons. The chains remain in the transconfiguration and can be looked upon as rigid molecules.

Orientation and strength of the electric-field-gradient (efg) tensors at the deuteron sites can be deduced from so-called rotation patterns. Above about 100 K, some molecular time-averaging processes take place and the mean efg parameters are averages of several sites.

These processes are well known from the literature.[10–13] A first averaging is due to a rapid exchange of deuterons in the ND_3 groups by jumpwise rotations around their threefold molecular axis. Hence, all three deuterons in a group see the same averaged efg tensor. The principle axis component V_{zz} of the efg tensor is measured along the axis of hindered rotation; it is nearly parallel to the C—N bond terminating the hydrocarbon chain. The second averaging process, which determines to a certain extent the symmetry of the crystal, is due to reorientational jumps of the molecules around their long axes between four positions with occupation probabilities n_1, n_2, n_3, and n_4.

The effect of these processes on the symmetry of PAMC can be summarized as follows: In the high-temperature α phase (space group $I4/mmm$) these four positions are equally populated ($n_1=n_2=n_3=n_4$) and the time-averaged long axis of the molecule is fourfold. In the partially ordered β and δ phases (*Cmca*) two of the orientations become nonequivalent in such a way that the time-averaged long axis is situated on a mirror plane (e.g., $n_1=n_2\neq n_3=n_4$). Finally a completely ordered state (i.e., one of the occupation numbers equals one, the others are zero) is reached below 115 K with the onset of the monoclinic ζ phase, as will be shown later. The exchange within the ND_3 group is still present at this stage, but dies out in the ζ phase around 100 K without affecting the symmetry of the crystal.

In the incommensurate γ phase the order parameter $n_1+n_2-(n_3+n_4)$ of the β phase is not or only slightly affected.[14] There is evidence that the incommensurate modulation originates from a rearrangement of the time-averaged longitudinal axes of the propylammonium (PA) groups. This rearrangement is due to a shrinking of the molecule diameter with lowering temperature and not directly related to the order parameter of the β phase.[15]

The kind of dynamics present in ϵ and ζ PAMC is still not exactly known. It is an open question whether the δ-ϵ transition is connected with any qualitative change of the chain dynamics. No explanation for the wave-vector switching at the ϵ-ζ transition has been given so far. The low-temperature phase sequence of PAMC cannot be described by pure order-disorder processes of the PA chains. This approach has been very successfully applied to other compounds of the $(C_nH_{2n+1}NH_3)_2MCl_4$ family investigated so far ($n<5$), where the sequential freezing out of the librational degrees of freedom of the chains leads to zone center or zone-boundary phase transitions.[11] In the case of PAMC some couplings between lattice modes and chain dynamics must play an important role.

The aim of the present work was to find out more about the chains dynamics and their relationship to lattice modulations. For this purpose measurements of pure chlorine NQR (Sec. III), quadrupole perturbed deuteron NMR (Sec. IV), second moment of protons (Sec. V), and elastic neutron scattering have been performed on partially deuterated crystals. In the last section couplings between lattice waves and orientational disorder of the chains are considered.

II. SYMMETRIES OF ϵ AND ζ PAMC

The phase sequence commonly observed in structurally incommensurate systems is as follows:[16] high-symmetry disordered phase (P) –incommensurate phase (I) –commensurate phase (C). The P-I transition is the result of a condensation of a soft mode with a wave vector $\mathbf{k}_0$ which is incommensurate with respect to the periodicity of the underlying lattice, whereas at the I-C transition the wave vector of the frozen-out modulation adopts a commensurate value $\mathbf{k}_c$, i.e., the average wave vector "locks in" to the basic lattice. A group-subgroup relation holds between the space groups of P (G_P) and C (G_C). The symmetry group of I is given by one of the irreducible repre-

sentations (reps) of G_P for $\mathbf{k}=\mathbf{k}_0$. The symmetry of the modulated crystal can also be defined in terms of the super-space groups.[17] Both descriptions contain the same information.

The space group of δ PAMC is *Cmca*. Its symmetry elements are listed in Table I. The ϵ phase is modulated along the a direction. The reps of interest are therefore those for k vectors on the Σ line. They are given in Table II. The three generating elements of the super-space group of ϵ PAMC above are

$$\begin{pmatrix} m \\ 1 \end{pmatrix} = \{\bar{m}_x \mid 000,0\}, \quad \binom{c}{1} = \{m_y \mid 0\tfrac{1}{2}\tfrac{1}{2},0\} ,$$

and

$$\binom{a}{s} = \{m_2 \mid \tfrac{1}{2}0\tfrac{1}{2},\tfrac{1}{2}\} ,$$

where the bar above m_x indicates the inversion of the fourth coordinate and s defines a translation of half a modulation wavelength. The elements m_y and m_z generate the symmetry-group $G(\Sigma)$ of the wave vector $\mathbf{k}_0=\sigma\mathbf{a}^*$. Hence, $\binom{c}{1}$ and $\binom{a}{s}$ define the symmetry of the soft mode. Comparison with Table II shows that the soft mode must have the symmetry of the Σ_3 representation $[\tau(g_{27})=1, \tau(g_{28})=-1]$.

It is not sure *a priori* that the general rule of the group-subgroup relation between G_P and G_C is applicable to ζ PAMC, because the modulation wave vector switches at the (first-order) ϵ-ζ transition. There is, however, strong experimental evidence that this relation nevertheless holds. The intensities of the neutron scattering Bragg peaks[3] reflect the temperature behavior of a slight first-order transition with a power law $[(T-T_c')/T_c']^{2\beta}$ with $\beta\simeq 0.20$ and $T_c'\simeq T_c+10$ K. The line splitting of the ^{35}Cl-NQR spectra exhibit the typical temperature dependence for phase transitions which can be described by an order parameter. It is therefore worthwhile to investigate the symmetry properties of soft modes of δ PAMC with a wave vector $\mathbf{k}_c=\mathbf{g}_1/3=(\mathbf{a}^*+\mathbf{b}^*)/3$ (or, equivalently, $g_2/3$). The star consists of the four vectors

TABLE I. Symmetry elements of the space group *Cmca*. The elements are numbered according to Kovalev (Ref. 19) and are given in the usual notation $\{R \mid \mathbf{t}\}$, where R is a point-group operation and t is a partial translation defined in the orthogonal basis of the nonprimitive unit cell in fractions of the lattice constants a, b, and c. The basic translations of the base centered lattice are $\mathbf{t}_1=(\mathbf{a}+\mathbf{b})/2$; $\mathbf{t}_2=(-\mathbf{a}+\mathbf{b})/2$; $\mathbf{t}_3=\mathbf{c}$. The basic vectors of the reciprocal lattice are $\mathbf{g}_1=\mathbf{a}^*+\mathbf{b}^*$; $\mathbf{g}_2=-\mathbf{a}^*+\mathbf{b}^*$, $\mathbf{g}_3=c^*$. For PAMC the dimensions of the unit cell are $a=7.169$ Å; $b=25.61$ Å; $c=7.458$ Å [δ phase, 182 K [(Ref. 18)].

$g_1=\{e/000\}$	$g_{25}=\{I/000\}$
$g_2=\{2_x/000\}$	$g_{26}=\{m_x/000\}$
$g_3=\{2_y/\tfrac{1}{2}0\tfrac{1}{2}\}$	$g_{27}=\{m_y/\tfrac{1}{2}0\tfrac{1}{2}\}$
$g_4=\{2_z/\tfrac{1}{2}0\tfrac{1}{2}\}$	$g_{28}=\{m_z/\tfrac{1}{2}0\tfrac{1}{2}\}$

$$\{\mathbf{k}_1=\mathbf{g}_1/3, \mathbf{k}_2=-\mathbf{k}_1, \mathbf{k}_3=\mathbf{g}_2/3, \mathbf{k}_4=-\mathbf{k}_3\}$$

and the only nontrivial element of the symmetry group $G(\zeta)$ of $\mathbf{k}_c$ is the glide reflection g_{28}. The basis of the irreducible representations ζ_1 and ζ_2, as introduced in Table III can be written as

$$Q(\mathbf{k}_1)=Q_1, \quad Q(\mathbf{k}_2)=Q_1^* ,$$

$$Q(\mathbf{k}_3)=Q_2, \quad Q(\mathbf{k}_4)=Q_2^* .$$

In order to find subgroups with the highest possible symmetry we have to look for invariant subspaces of the representation space. As we are only interested in the case with the average values $\langle Q_1\rangle\neq 0$ and $\langle Q_2\rangle=0$, this subspace is included in the space $\{Q_1, Q_1^*\}$, which is left invariant by the elements g_1, g_4, g_{25}, and g_{28}, as can be derived from Table III. Only elements with real representations can be conserved. The largest possible group of ζ PAMC is therefore $\{g_1, t_1\cdot g_4, g_{25}, t_1\cdot g_{28}\}$, where t_1 is understood to be the basic translation $\{e \mid \tfrac{1}{2}\tfrac{1}{2}0\}$. This group has four one-dimensional reps, which are all induced by ζ_1 and ζ_2 in the real basis $\{(Q_1+Q_1^*)/\sqrt{2},$

TABLE II. Irreducible representations on the Σ line at $\mathbf{k}_0=\sigma\mathbf{a}^*$ $(0<\sigma<\tfrac{1}{2})$ with $\epsilon=\exp(-i\pi\sigma)$. The star consists of the two vectors $\{\mathbf{k}_1=\mathbf{k}_0, \mathbf{k}_2=-\mathbf{k}_0\}$ and is generated by g_1 and g_{25}, for instance. The symmetry group $G(\Sigma)$ of $\mathbf{k}_0$ is $\{g_1, g_2, g_{27}, g_{28}\}$. The small representations are obtained as shown in the lower table (after Ref. 19).

g	1	2	3	4	25	26	27	28
Σ_1	$\begin{pmatrix}1&0\\0&1\end{pmatrix}$	$\begin{pmatrix}1&0\\0&1\end{pmatrix}$	$\begin{pmatrix}0&\epsilon\\\epsilon^*&0\end{pmatrix}$	$\begin{pmatrix}0&\epsilon\\\epsilon^*&0\end{pmatrix}$	$\begin{pmatrix}0&1\\1&0\end{pmatrix}$	$\begin{pmatrix}0&1\\1&0\end{pmatrix}$	$\begin{pmatrix}\epsilon&0\\0&\epsilon^*\end{pmatrix}$	$\begin{pmatrix}\epsilon&0\\0&\epsilon^*\end{pmatrix}$
Σ_2	+	+	−	−	+	+	−	−
Σ_3	+	−	+	−	+	−	+	−
Σ_4	+	−	−	+	+	−	−	+

g	1	2	27	28
τ_1	1	1	ϵ	ϵ
τ_2	1	1	$-\epsilon$	$-\epsilon$
τ_3	1	−1	ϵ	$-\epsilon$
τ_4	1	−1	$-\epsilon$	ϵ

TABLE III. Irreducible representations for a general wave vector $\mathbf{k}_1=\mu_1\mathbf{g}_1+\mu_2\mathbf{g}_2$ in the $(\mathbf{a}^*,\mathbf{b}^*)$ plane. E, A, B, C are the following two-dimensional matrices: $E=\begin{pmatrix}1&0\\0&1\end{pmatrix}$, $A=\begin{pmatrix}0&1\\1&0\end{pmatrix}$, $B=\begin{pmatrix}\epsilon&0\\0&\epsilon^*\end{pmatrix}$, $C=\begin{pmatrix}0&\epsilon\\\epsilon^*&0\end{pmatrix}$, where $\epsilon=\exp[-i\pi(\mu_1-\mu_2)]$. The star consists of the four vectors $\mathbf{k}_1$, $\mathbf{k}_2=-\mu_1\mathbf{g}_1-\mu_2\mathbf{g}_2$, $\mathbf{k}_3=\mu_2\mathbf{g}_1+\mu_1\mathbf{g}_2$, and $\mathbf{k}_4=-\mu_2\mathbf{g}_1-\mu_1\mathbf{g}_2$. As generating elements of the star one can take g_1, g_{25}, g_{26}, and g_2. ζ_1 has the trivial small loaded representation.

g	1	2	3	4	25	26	27	28
ζ_1	$\begin{pmatrix}E&0\\0&E\end{pmatrix}$	$\begin{pmatrix}0&A\\A&0\end{pmatrix}$	$\begin{pmatrix}0&B\\B^*&0\end{pmatrix}$	$\begin{pmatrix}C&0\\0&C^*\end{pmatrix}$	$\begin{pmatrix}A&0\\0&A\end{pmatrix}$	$\begin{pmatrix}0&E\\E&0\end{pmatrix}$	$\begin{pmatrix}0&C\\C^*&0\end{pmatrix}$	$\begin{pmatrix}B&0\\0&B^*\end{pmatrix}$
ζ_2	+	+	−	−	+	+	−	−

$(Q_1-Q_1^*)/\sqrt{2}\}$. The result is shown in Table IV together with the possible space groups of ζ PAMC and the number of the corresponding chlorine sites.

The experimentally observed number of chemically inequivalent chlorine sites is 6 (Fig. 3) and one can conclude that ζ PAMC has a space group $P112_1/n$ with the elements g_1, $g_4=\{2_z \mid 1\frac{1}{2}\frac{1}{2}\}$, g_{25}, and $g_{28}=\{m_z \mid 1\frac{1}{2}\frac{1}{2}\}$. As new basis vectors of the lattice one can choose $\mathbf{a}'=3\mathbf{t}_1-\mathbf{t}_2=2\mathbf{a}+\mathbf{b}$, $\mathbf{b}'=\mathbf{t}_2$, and $\mathbf{c}'=\mathbf{c}$ and the symmetry elements appear in standard notation for $P112_1/a$: $g_4=\{2_z \mid \frac{1}{2}0\frac{1}{2}\}$ and $g_{28}=\{m_z \mid \frac{1}{2}0\frac{1}{2}\}$. The new basis of the reciprocal lattice is

$$\{\mathbf{g}_1'=\mathbf{g}_1/3, \mathbf{g}_2'=\mathbf{g}_2+\mathbf{g}_1/3, \mathbf{g}_3'=\mathbf{g}_3\} .$$

It is noteworthy that ζ_2 and Σ_3 are compatible with each other. Σ_3 and Σ_2 are obtained from ζ_2 in the basis

$$\{(Q_1+Q_2^*)/\sqrt{2}, (Q_1^*-Q_2)/\sqrt{2}, (Q_1-Q_2^*)/\sqrt{2}, (Q_1^*-Q_2)/\sqrt{2})\} .$$

A schematic drawing of ζ PAMC is shown in Fig. 1(b). The modulation leaves the inversion centers (g_{25}) at the corners of the new unit cell.

In order to understand the D-NMR spectra it is necessary to introduce the unit cell of δ PAMC in more detail. If the PA chains are considered as rigid bodies, the structure of δ PAMC has four sublattices: the manganese sites, the in-plane chlorine sites [Cl.(1)], the out-of-plane chlorine sites [Cl(2)], and the PA sites (A) (Fig. 2). The site numbers given in Fig. 2 are the same as in Ref. 20.

III. PURE ^{35}Cl-NQR

In spite of the large anomalous broadening of the chlorine-NQR signals due to the incommensurate modulation, it was possible to detect the chlorine signals in the ϵ phase by a pulse technique (Fig. 3). The spectral lines are broadened over a range of up to 500 kHz in case of the in-plane Cl nuclei [Cl(1) site], and up to 80 kHz in case of the out-of-plane nuclei [Cl(2) site]. With lowering temperature the Cl(1) spectra shows more structure than the usual edge singularities, probably due to solitonlike distortions of the incommensurate modulation. Below T_c the number of spectral lines is triplicated with respect to the number in the δ phase. The line splitting in function of temperature is continuous at the δ-ϵ transition (second order) and discontinuous at the ϵ-ζ transition (first order), confirming previous determinations of the order of the phase transitions.[3,8]

The NQR frequency is a function of the charge density $\rho(r)$. At a continuous phase transition ρ will experience a change $\delta\rho\equiv\rho(\eta)-\rho_0$, $\rho_0\equiv\rho(\eta=0)$, which depends in first approximation only on the order parameter η. Lan-

TABLE IV. Irreducible representations ζ_1 and ζ_2 of the subgroup $\{g_1, t_1g_4, g_{25}, t_1g_{28}\}$ in the basis (a) Q_1, Q_1^* (obtained from Table III); (b) $(Q_1+Q_1^*)/\sqrt{2}$, $(Q_1-Q_1^*)/\sqrt{2}$. The possible space groups for ζ PAMC and the corresponding number of chemically inequivalent chlorine sites in the unit cell are given in the last two columns.

	g_1	t_1g_4	g_{25}	t_1g_{28}	Space group	Number of Cl sites
			(a)			
ζ_1	$\begin{pmatrix}1&0\\0&1\end{pmatrix}$	$-\begin{pmatrix}0&1\\1&0\end{pmatrix}$	$\begin{pmatrix}0&1\\1&0\end{pmatrix}$	$-\begin{pmatrix}1&0\\0&1\end{pmatrix}$		
ζ_2	$\begin{pmatrix}1&0\\0&1\end{pmatrix}$	$\begin{pmatrix}0&1\\1&0\end{pmatrix}$	$\begin{pmatrix}0&1\\1&0\end{pmatrix}$	$\begin{pmatrix}1&0\\0&1\end{pmatrix}$		
			(b)			
ζ_1	1	−1	1	−1	$P1$	12
	1	1	−1	−1	$P112_1$	12
ζ_2	1	1	1	1	$P112_1/n$	6
	1	−1	−1	1	$P11n$	12

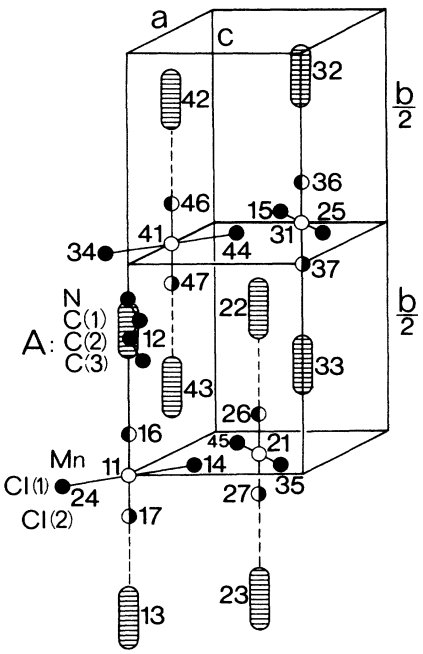

FIG. 2. Schematic picture of the structure of PAMC in the nonprimitive unit cell.

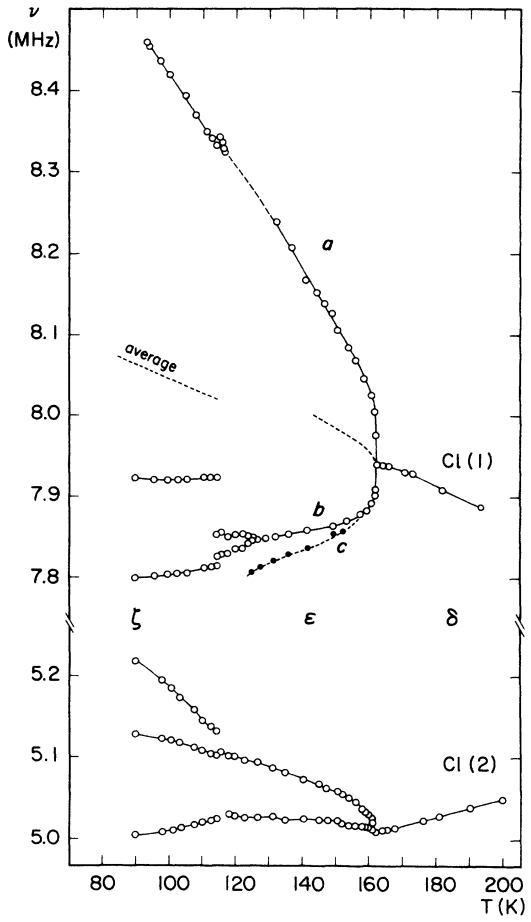

FIG. 3. Pure ^{35}Cl-NQR frequencies vs temperature. The sample was composed of large single crystals with a total volume of about 1.5 cm^3. The signals were accumulated between 20 000 and 100 000 times. The frequency averages of the Cl(1)-NQR lines are indicated by broken lines. The solid circles stand for one of the two-edge singularities.

dau and Lifshitz[21] have shown that $\delta\rho$ can be expanded in terms of the order parameter as follows:

$$\delta\rho=\eta\cdot\sum\gamma_i\psi_i\ (+\ \text{higher-order terms})\ , \tag{1}$$

where ψ_i are the basis functions of an irreducible representation and the coefficients γ_i are the normalized components of the order parameter ($\sum\gamma_i^2=1$).

Expanding the NQR frequency deviation $\Delta\nu=\nu(\rho_0+\delta\rho)-\nu(\rho_0)$ around $\rho=\rho_0$ up to second order in powers of $\delta\rho$, the change of frequency $\Delta\nu(s)$ in function of η for a nucleus at site s is obtained as in[22]

$$\Delta\nu=\eta\sum_i\gamma_i\frac{\partial\nu(s)}{\partial\psi_i}\bigg|_{\eta=0}+\tfrac{1}{2}\eta^2\sum_{i,j}\gamma_i\gamma_j\frac{\partial^2\nu(s)}{\partial\psi_i\partial\psi_j}\bigg|_{\eta=0}\ . \tag{2}$$

As basis functions ψ_i, one can take the coordinates of symmetry adapted basis vectors. The ψ_i occurring in the linear term must have the symmetry of one of the irreducible representations contained in the equivalent site representation defined by the sublattice with site s. The latter representation is a regular one and consists of the matrices obtained by permuting the sites of a given sublattice under the operation of the symmetry group $G(k)$ of the wave-vector k of the soft mode. This means that $\nu(s)$ cannot linearly depend on those distortions that destroy the point symmetry of the site s. This result can be obtained by simpler argumentation, especially for Γ-point transitions.[23] It has to be kept in mind, however, that the relevant point symmetry must be a subgroup of $G(k)$.

The point symmetry of the Cl(1) site is 2_y. This element is not contained in $G(\Sigma)=\{e,2_x,m_y,m_z\}$ nor in $G(\zeta)=\{e,m_z\}$ [symmetry group of a wave vector in the (k_x,k_y) plane]. The first-order term of Eq. (2) therefore exists in the ϵ as well as in the ζ phase and $\Delta\nu$[Cl(1)] should depend linearly on η.

Denoting the sites in the enlarged unit cell of the ζ phase as s at $r(s)$, s' at $r(s)+t_1$, and s'' at $r(s)+2t_1$, where s is a site of the δ phase, and taking them as basis of the equivalent site representation, we find that there are three subspaces of Cl(1), $S_0=\{14,24,45',35''\}$, $S_1=\{14',24'',45'',35'\}$, and $S_2=\{14'',24',45,35\}$, which are invariant under the symmetry operations of the ζ phase. All irreducible Γ point representations of $P112_1/n$ occur just once in each subspace. It follows that the Cl(1) spectrum consists of three lines (as was deduced before), for there are as many lines as the unity representation occurs.[22] Thus $\Delta\nu$ of a nucleus in the lth unit cell at site s depends linearly on the displacements

$$\mathbf{u}(l,s)=Q_{\mathbf{k},j}\cdot\mathbf{e}(\mathbf{k}j\mid s)\cdot e^{i\mathbf{k}\mathbf{r}(l,s)}+\text{c.c.} \tag{3}$$

The relationship between the frequencies of the three subspaces are obtained from expression (3) as $\nu(S_n)=\Delta\nu(S_0)\cos(\phi_0+n\cdot2\pi/3)$ in first approximation,

as the derivative $\partial\nu(s)/\partial\psi_i$ is proportional to the same phase factor $\cos[\phi_i(s)+1\cdot 2\pi/3]$ for all i. Summarizing, the following relations hold if the temperature dependence of the spectra is governed completely by the linear term in expression (2):

$$\nu(\eta,n)=\nu(\eta=0)+\Delta\nu(S_0,\eta)\cdot\cos(\phi_0+n\cdot 2\pi/3)\ , \tag{4a}$$

$$\sum_n \Delta\nu(S_n)=0\ , \tag{4b}$$

$$\Delta\nu(S_0,\eta)=\eta\cdot\text{const}\ , \tag{4c}$$

$$\langle\nu(\eta)\rangle\equiv\frac{1}{n}\sum_n\nu(\eta,n)=\nu(\eta=0)\ . \tag{4d}$$

$\nu(\eta=0)$ is the extrapolated frequency of the high-symmetry phase. Equation (4a) is almost exactly fulfilled in case of the Cl(1) nuclei with a phase angle ϕ_0 of $10°\pm 1°$. There is only a constant offset between $\nu(\eta=0)$ and $\langle\nu(\eta)\rangle$ of 20 kHz [$=5\%$ of $\Delta\nu(S_0,\eta)=380$ kHz at 100 K].

In the incommensurate ϵ phase the frequency distribution is a quasicontinuum, because the phase in Eq. (4a) is not incremented by a rational fraction of 2π. Equation (4a) is valid in the form

$$\nu(\eta)=\nu(\eta=0)+\alpha\eta\cos(\Phi)\ , \tag{5}$$

where Φ takes all possible values. In the plane-wave limit, all Φ occur with the same probability and the observable edge singularities take the values $\Phi=0$ and $\Phi=\pi$.[24] Hence, the average frequency of the edge singularities should be equal to $\nu(\eta=0)$ in first approximation. The observed difference is about 20 kHz at 150 K ($\simeq 8\%$ of the line splitting). The frequency difference $\nu(\eta,0)-\nu(\eta,\pi)$ is therefore proportional to η in good approximation. The critical exponent β of the order parameter is obtained as $\beta=0.37\pm 0.03$ (see Fig. 4). As soon as the modulation wave is distorted, certain phases Φ occur preferentially and other types of singularities appear (the "forerunners" of commensurate ordering at lower temperatures), owing to the fact that several translational domains may occur. This is also observed in the Cl(1) spectrum, where the singularity b (see Fig. 3) is split into two parts between T_c and 125 K. These lines correspond to phase angles Φ of approximate $\pm 2\pi/3$, which is near to the values observed in ζ PAMC. They develop continuously out of the edge singularity for $\Phi=\pi$ (line c). The observed phase values also explain the higher intensity of singularity b with respect to singularity a, since the relative weight of the first line increases from about $\frac{1}{2}$ continuously to $\frac{2}{3}$, whereas the relative weight of the latter decreases. This fact also makes it impossible to find the true average frequency in the lower half of the ϵ phase. The edge singularity for $\Phi=0$ (line a) must be almost identical to the commensurate line. In the temperature range where the "commensurate" lines start to appear, line a could not be observed (broken line in Fig. 3). The edge singularity for $\Phi=\pi$ (line c) can be observed as a diminishing shoulder on the low-frequency side of singularity b.

In most cases the additional singularities of the line shape can be derived from the lowest-order Cl term of the order parameter. In our case [$\mathbf{k}_0=\frac{1}{6}(\mathbf{g}_1-\mathbf{g}_2)$], this term is of order 6, i.e., proportional to $\cos(6\phi)$. Hence, the phase difference between translational domains should be a multiple of $2\pi/6$, and not $2\pi/3$ as observed. Our experimental finding indicates that the lowest-order U term in the free-energy density must be a third-order term in η multiplied by another independent parameter of appropriate symmetry.

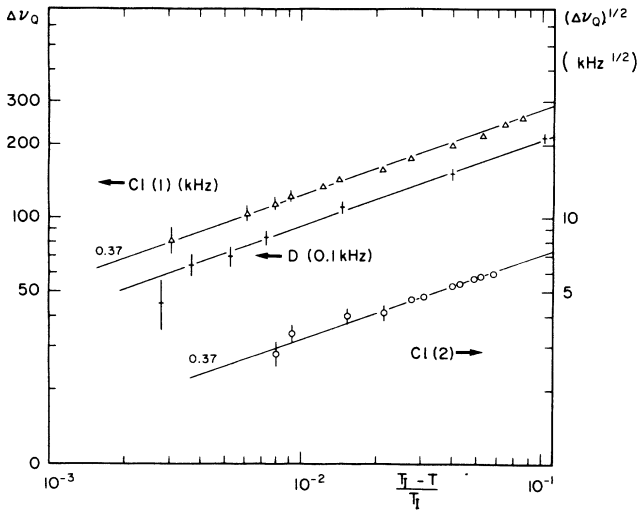

FIG. 4. Log-log plot of the amplitude of the NQR line splitting vs normalized temperature difference to T_I. △: $\Delta\nu_Q$ of pure ^{35}Cl-NQR of the Cl(1) site, $\beta=0.37\pm 0.03$ (left-hand scale in units of kHz). +: Quadrupole perturbed D-NMR with the magnetic field B_0 (1.600 T) in the (a,b) plane, $(\mathbf{B}_0,\mathbf{b})=60°$, $\beta=0.38\pm 0.04$ (left-hand scale in units of 0.1 kHz). ○: $(\Delta\nu_Q)^{1/2}$, i.e., the square root of the splitting of pure ^{35}Cl-NQR lines of the Cl(2) site, $\beta=0.34\pm 0.03$ (right-hand scale).

The same considerations as made above are also valid for the Cl(2) site, i.e., that the frequency difference $\Delta\nu(s)$ should be a linear function of the order parameter in first approximation. The measurements show, however, a completely different behavior. The terms quadratic in η are obviously much larger than the linear terms. This becomes evident from a comparison of the average frequency of the ϵ phase with the extrapolated $\nu(\eta=0)$. The critical exponent 0.68 ± 0.03 of the frequency splitting above 154 K is nearly two times larger as the one determined from the Cl(1) spectra (Fig. 5). Below 154 K, however, the exponent measured as $\beta\simeq 0.4$ is rather the same as deduced from the Cl(1) spectra. This strange behavior must be due to a second kind of ordering process connected with the incommensurate modulation. The NQR frequency of Cl(2) nuclei is obviously an even function of the order parameter p of this second process. As a consequence, the latter must have the symmetry of such a Γ-point or Y-point representation which leads to a destruction of the mirror plane m_x (in principle, p could be modulated in the y and z directions, but this makes no sense). The large contribution of p to the NQR spectrum of the Cl(2) site makes clear that the ordering associated with p is not only a secondary effect, but must be one of the leading mechanisms making the crystal unstable with

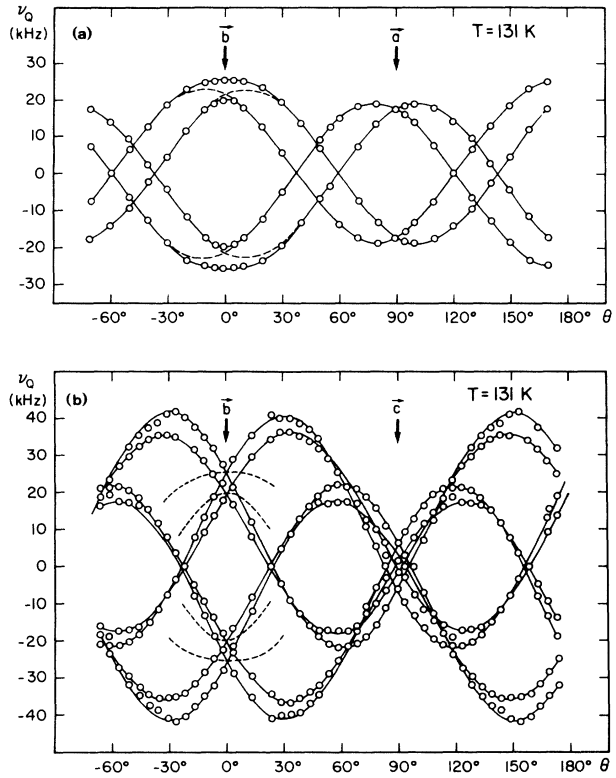

FIG. 5. Quadrupolar splitting of D-NMR as a function of the rotation angle θ. External magnetic field: 1.600 T; $\nu=10.4$ kHz; $T=131$ K (ϵ phase). (a) Rotation of the field in the (a,b) plane. The broken lines around $\theta=0$ indicate the unobserved crossings of the lines with constant modulation phase angles of $\pm\pi/2$. (b) Rotation of the field in the (b,c) plane. The broken lines are from (a) for comparison.

respect to an incommensurate modulation. There is apparently no distortion of the anorganic layer with the symmetry of this second-ordering process, because it does not influence the efg tensor at the Cl(1) site. Hence, the second process must be connected with the freezing of the flipping motions of the PA chains. It is clear that the orientation of the ammonium heads affects the Cl(2) spectra much more than the Cl(1) spectra.

IV. QUADRUPOLE PERTURBED D-NMR

D-NMR at partially deuterated crystals allows us to measure the time-averaged directions of the C—N bonds terminating the chains. A change of orientation of the efg tensors at the D sites is due to either a rotation of the molecule or a change of the occupation probabilities n_1-n_4 of the four orientational positions. Hence, amplitudes of rotational components of a frozen-out mode can be measured directly, provided that the two contributions can be separated. This separation was possible in case of γ PAMC.[14]

At the ϵ-ζ transition the order parameter $(n_1+n_2)-(n_3+n_4)$ of the order-disorder β-α transition is saturated (see the Introduction). In time average the PA chains are situated an a mirror plane m_x. The largest component $V^p_{zz}\equiv eq$ of the efg tensor is measured in the direction of the average C—N bond. The corresponding principle axis and the layer normal (b axis) include an angle of $\alpha_0=31°$ at 173 K.[14] The principle axis with the smallest component $V^p_{xx}\equiv-\frac{1}{2}(1-\tilde{\eta})eq$ stays perpendicular to the mirror plane m_x. Measurements yielded a quadrupole coupling constant e^2qQ/h of (50.1 ± 0.5) kHz and an asymmetry parameter $\tilde{\eta}$ of 0.04 ± 0.02 at 173 K.[14] In the crystal frame with x along **a**, y along **b**, and **z** along c, the two inequivalent efg tensors (V^0) at the D sites occurring in the unit cell of δ PAMC read as the following:

$$\begin{aligned}
V^0_{zz}&=V^p_{yy}+(V^p_{zz}-V^p_{yy})\sin^2\alpha_0\ ,\\
V^0_{yy}&=V^p_{zz}-(V^p_{zz}-V^p_{yy})\sin^2\alpha_0\ ,\\
V^0_{xx}&=V^p_{xx}\ ,\\
V^0_{yz}&=\pm\tfrac{1}{2}(V^p_{zz}-V^p_{yy})\sin(2\alpha_0)\ ,\\
V^0_{xy}&=V^0_{xz}=0\ .
\end{aligned}\tag{6}$$

In ϵ and ζ PAMC the efg tensors are tilted around all crystallographic axes. In first approximation the changes of the efg tensors (V) can be written as a linear superposition of rotations (rotation matrix R) around all three axes:

$$\begin{aligned}
V-V^0=&R_x^T(\alpha)\cdot V^0\cdot R_x(\alpha)+R_y^T(\beta)\cdot V^0\cdot R_y(\beta)\\
&+R_z^T(\gamma)\cdot V^0\cdot R_z(\gamma)-3V^0\ .
\end{aligned}\tag{7}$$

The modulated tilt angles of the PA chains (sublattice A) are described by the rotational part d of the polarization vector. For the ϵ phase (wave-vector **k**, rep Σ_3) d is obtained as

$$\begin{aligned}
d(\mathbf{k},\Sigma_3\mid A)=&a_1\cdot R_x\mid A_2\rangle+ib_2\cdot R_y\mid A_1\rangle\\
&+ib_3\cdot R_z\mid A_3\rangle\ .
\end{aligned}$$

$\mid A_i\rangle$ denotes the basis vectors of the reduced equivalent site representation for $\mathbf{k}=0$. On the basis of the D sites $\mid 12\rangle$, $\mid 13\rangle$, $\mid 22\rangle$, $\mid 23\rangle$, they have the components

$$\begin{aligned}
&\mid A_1\rangle=(1,1,1,1),\quad \mid A_2\rangle=(1,-1,1,-1)\ ,\\
&\mid A_3\rangle=(1,1,-1,-1),\quad \mid A_4\rangle=(1,-1,-1,1)\ .
\end{aligned}$$

Time-reversal symmetry requires $d^*(\bar{A})=-d(A)$, where $\bar{A}$ denotes the configuration after inversion operation.[25] The coefficients a_i and b_i are real by this property. Introducing the normal coordinate $\frac{1}{2}\eta\exp(i\Phi_0)$ the tilt angles at the site c in the lth unit cell are obtained as

$$\begin{aligned}
\alpha(\Sigma_3,l,c)&=\eta a_1\cos\Phi(l,c)\mid A_2\rangle_c\ ,\\
\beta(\Sigma_3,l,c)&=-\eta b_2\sin\Phi(l,c)\mid A_1\rangle_c\ ,\\
\gamma(\Sigma_3,l,c)&=-\eta b_3\sin\Phi(l,c)\mid A_3\rangle_c\ .
\end{aligned}\tag{8}$$

The phase angle Φ is defined as $\Phi(l,c)=\Phi_0+\mathbf{k}_0\mathbf{r}(l,c)$. In the ζ phase additional rotations occur. These have the Σ_2 symmetry. The corresponding angles are

$$\alpha(\Sigma_2,l,c)=-\eta b_1\sin\Phi(l,c)\,|\,A_1\rangle_c\ ,$$
$$\beta(\Sigma_2,l,c)=\eta a_2\cos\Phi(l,c)\,|\,A_2\rangle_c\ , \qquad (9)$$
$$\gamma(\Sigma_2,l,c)=\eta a_3\cos\Phi(l,c)\,|\,A_4\rangle_c\ .$$

The modulation phase angle is $\Phi=\Phi_0+\mathbf{k}_0\mathbf{r}(l,c)$. Whereas, Φ_0 has an arbitrary value in the ϵ phase, it has a defined value in the ζ phase depending on the coordinates of the inversion center. In the δ phase two types of inversion centers exist: one in the Mn sites ($\mathbf{r}=\mathbf{0}$) and one in the middle between two Mn sites ($\mathbf{r}=\mathbf{t}_1/2$). In the ζ phase both types of inversion centers occur. Choosing a translational domain with the conserved inversion center at $\mathbf{r}=\mathbf{0}$, the second type of inversion center has the coordinates $\frac{1}{2}\mathbf{t}_1$ and Φ_0 amounts to $\pm\pi/2$. This value is derived from the condition that rotation angles do not change sign under the inversion operation.

The rotation patterns of the ϵ phase (Fig. 5) show that V_{xx} is independent of Φ. The change of V_{xx} caused by the tilt angles according to Eq. (7) is obviously compensated by a modulation of the strength (eq) and the asymmetry ($\tilde{\eta}$) of the efg tensor. We further observe that the curves of Fig. 5(a) have a 2π periodicity, which is impossible for a NQR line of a single nucleus. Hence, we do not detect singularities with a constant Φ for all values of the rotation angle θ as in the case of γ PAMC. This fact has the following explanation. For θ between about 30° and 60°, the component V_{xy} with the linear contribution,

$$\tfrac{1}{2}(V^0_{yy}-V^0_{xx})\sin2\gamma\simeq-\eta(V^0_{yy}-V^0_{xx})b_3\sin\Phi$$

is the leading term and the observed edge singularities occur for $\Phi=\pm\pi/2$. At $\theta=0$, the component V_{yy} with the linear part

$$V^0_{yz}\sin2\alpha\simeq-2V^0_{yz}\eta a_1\cos\Phi$$

determines the maximum value of the splitting. Here the edge singularities occur for $\Phi=0$ and $\Phi=\pi$. Around $\theta=0$ the phase of the observed sites therefore changes from $-\pi/2$ to $+\pi/2$ via 0 or π. This property is nicely illustrated in Fig. 6 where calculated patterns are shown.

The rotation patterns of the ζ phase (Figs. 7 and 8) are compatible with the space group $P112_1/n$. If the field is rotated in the mirror glide plane from each domain, three lines are observed which are related to each other by the lost mirror plane m_x, for instance (Fig. 7). Rotating the field around the a axis, all six lines of a single domain can be observed. The pattern is symmetrical about the b axis. The signals from the two domains coincide (Fig. 8).

In Fig. 6 calculated rotation patterns are shown. Various simplifications were made. The curves are only approximate fits to the experimental data and should illustrate the main features of the patterns. In both patterns b_3 is the largest component of the polarization vector, i.e., the tilt angle γ has a much larger amplitude than α or β. This must be due to the freezing of the librational movements of the propylammonium chains, which causes a tilting of the molecules around the c axis. For a good fit to experimental data, it was necessary to also allow modulated asymmetry parameters and coupling strengths. In Fig. 6 a modulation of eq was needed in order to keep V_{xx} constant.

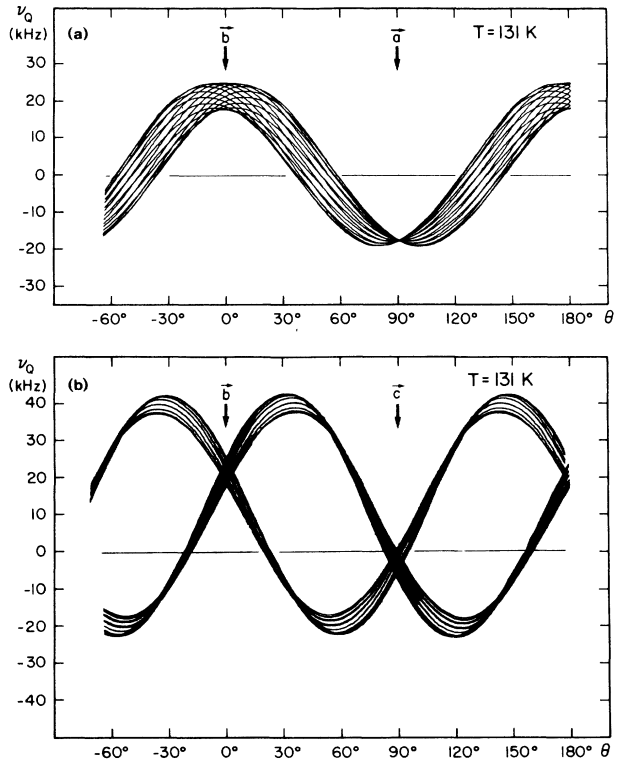

FIG. 6. Calculated D-NMR rotation patterns of the ϵ phase for different values of the phase angle $\phi=n\pi/8$ ($n=0.15$). $a_1=0.21$, $b_2=0$, $b_3=0.98$, $\eta=11°$, $V_{11}=-17.86$ kHz, $\tilde{\eta}=0.06-0.08\cos\phi$, and $e^2qQ/h(\phi=0)=51.1$ kHz. (a) (a,b) plane; (b) (b,c) plane.

In the case of ζ PAMC the rotation of the N—C bond cannot be correctly described by a sinusoidal modulation through the crystal. An approximate fit to Eqs. (8) and (9) yielded the values $a_1=b_2=0.06$, $b_3=0.996$, $a_2=a_3=b_1=0$, $e^2qQ/h=(57.6-1.9\times10^{-2}\gamma^2)$ kHz (γ in degrees), and $\tilde{\eta}=0.12-5\times10^{-4}\gamma^2$, $\eta=20°$.

In the temperature interval between the lock-in transition and about 122 K, the frequency distribution of D-NMR indicates solitonlike distortions. At least two additional weak lines appear between the two edge singularities.

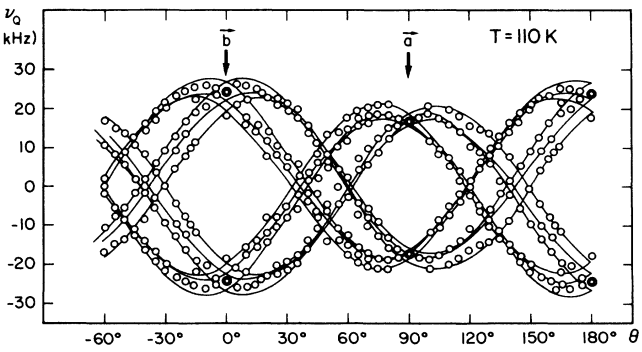

FIG. 7. D-NMR rotation pattern at $T=110$ K (ζ phase). The field rotates in the (a,b) plane.

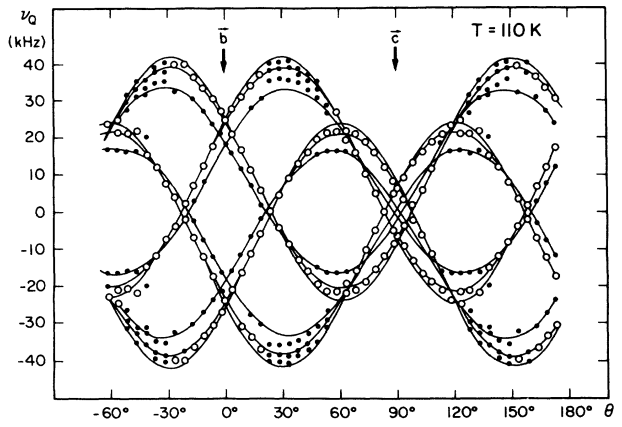

FIG. 8. *D*-NMR rotation pattern at $T=110$ K (ζ phase). The field rotates in the (b,c) plane.

V. SECOND MOMENT OF PROTON LINE SHAPES

In Ref. 3 it was suggested that the lock-in transition at 114.5 K is connected with the freezing of the dynamical disorder of the propyl-ammonium groups and/or of the NH_3 rotational movements. The latter mechanism can be excluded, because this movement is still present below this transition and averages the deuteron signals from the same ND_3 group. In order to obtain information about the first mechanism, the second moment M_2 of the proton magnetic resonance line shape was determined as a function of temperature. The time-resolved line shapes were measured with the help of the "solid echo" method. The pulse sequence used was a 1.8-μs-long 90° pulse followed by a $\pi/2$ phase-shifted 90° pulse after 40 μs. An increase of M_2 below $T=114.5$ K is indeed observed (Fig. 9). A recent Raman scattering experiment also leads to the conclusion that the dynamics of the chains freezes in at the ϵ-ζ transition.[26]

VI. NEUTRON SCATTERING

Elastic neutron scattering measurements (wavelength 2.34 Å) have been performed on a single crystal with dimensions $20\times20\times5$ mm^3 in the temperature range between 110 and 200 K. Previous data[3,8] about modulation and lock-in wave vectors have been confirmed. In addition, strong critical scattering of the satellite reflexions in the ϵ phase could be observed (Fig. 10). Their intensity in the function of temperature follows a logarithmic rather than a power law. This may indicate the vicinity of a tricritical point. The critical exponent β derived from the intensities of satellite reflexions (Fig. 7) is obtained as $\beta=0.43\pm0.03$.

For the partially deutered compound, the values of the incommensurate part $\delta\mathbf{a}^*$ of the modulation wave vector slightly departs from the ones of the nondeuterated compound (Fig. 11). δ has an interesting temperature behavior. In contrast to other incommensurate compounds with $\mathbf{k}_0=(1/3+\delta)\mathbf{a}^*$ and an anisotropy energy of sixth order in η, as K_2SeO_4 and Rb_2ZnCl_4,[27] where $d^2\delta/dT^2$ is negative in the hole incommensurate phase, in PAMC $d^2\delta/dT^2$ is positive for $140<T\leq T_I$ (Fig. 11).

There are other compounds with $d^2\delta/dT^2>0$. These are the charge-density wave systems 2H-$TaSe_2$ and 2H-$NbSe_2$ (Ref. 28) with $\mathbf{k}_0=(1/3-\delta)\mathbf{a}^*$ and an anisotropy energy of *third* order in η! Hence, consistently with NQR results we must assume the existence of a third-order lock-in term ($\eta^3+\eta^{*3}$).

As shown in the Appendix, $\delta(T)$ depends as $\delta(T)=\delta_0(1-\alpha r^{2n-4})$ on the amplitude r of the order parameter, where $\delta_0=\delta(T_I)$ and n the order of the Umklapp term. The order parameter varies as $(T_I-T)^\beta$ and $d^2\delta/dT^2$ is positive for $n<2+1/2\beta$. Taking a realistic value of $\beta=0.35$ the sign of curvature changes at $n=3,4$.

For $n=3$ one should obtain

$$\delta(T)=\delta_0[1-\alpha(T_I-T)^{2\beta}] .$$

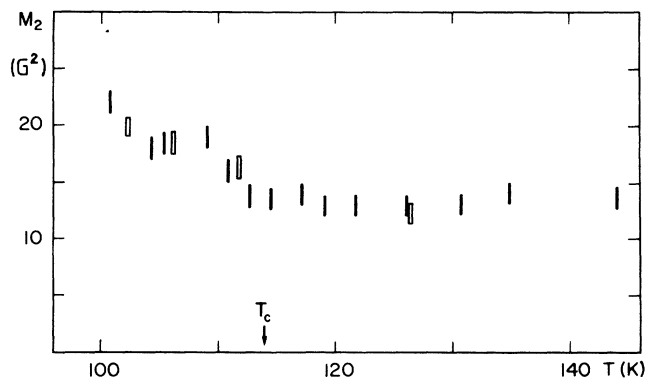

FIG. 9. Second moment of proton line shape vs temperature measured in a magnetic field of 0.38 T at 16.1 MHz. Solid bars: cooling; open bars: heating.

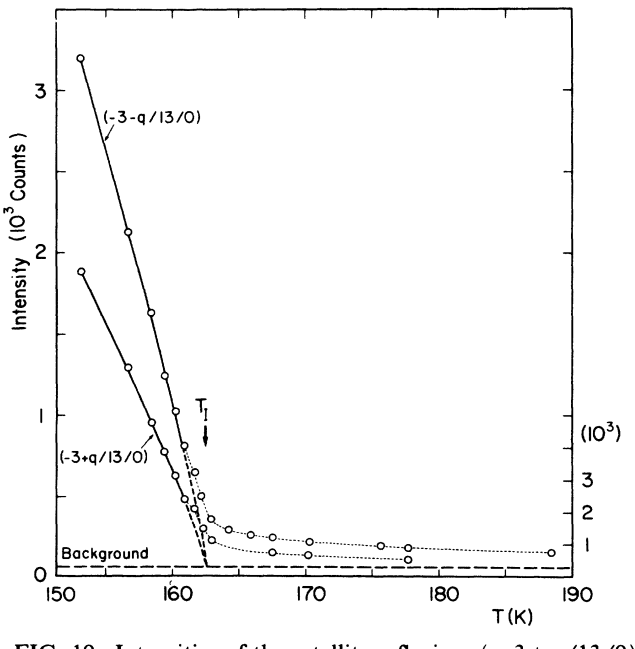

FIG. 10. Intensities of the satellite reflexions $(-3+q/13/0)$ and $(-3-q/13/0)$ vs temperature ($q=1/3+\delta$). The solid lines describe a power law $I=(T_I-T)^{0.85}$. The dotted lines are guides for the eye. For points above T_I the right-hand scale applies (longer integration time).

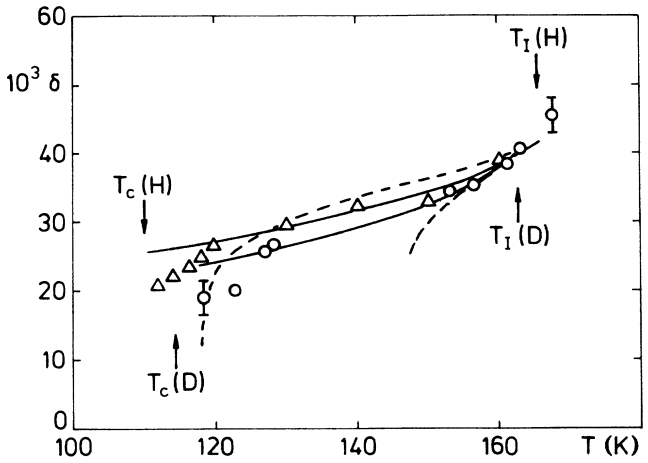

FIG. 11. The irrational part δ of the modulation wave vector $(1/3+\delta)\mathbf{a}^*$ in function of temperature. △: normal PAMC after Refs. 3 and 8. ○: partially deuterated PAMC. The values have been obtained from the satellite pair of Fig. 10. The solid and broken lines are described in the text.

The curve drawn in Fig. 11 has the parameters $2\beta=0.70$, $\delta 0=0.04$, $\alpha=0.030$ for the partially deuterated compound. The curve for the undeuterated compound has the parameters $2\beta=0,70$, $\delta_0=0.042$, $\alpha=0.025$.

The exact evaluation of the integral equation given in the Appendix shows, however, that the simple power law given above is valid in the vicinity of T_I only. A fit to the experimental data requires a temperature dependent γ/λ, where γ is the coefficient of the third-order lock-in term and λ the coefficient of the stabilizing term. If the order parameter is assumed as $\{(T_I-T)/T_I\}^{0.37}$, the ratio γ/λ varies between 1.4 at T_I and 0.8 at T_C. The broken lines in Fig. 11 show the calculated behavior of $\delta(T)$ for $\gamma/\lambda=1.3$ and 0.9.

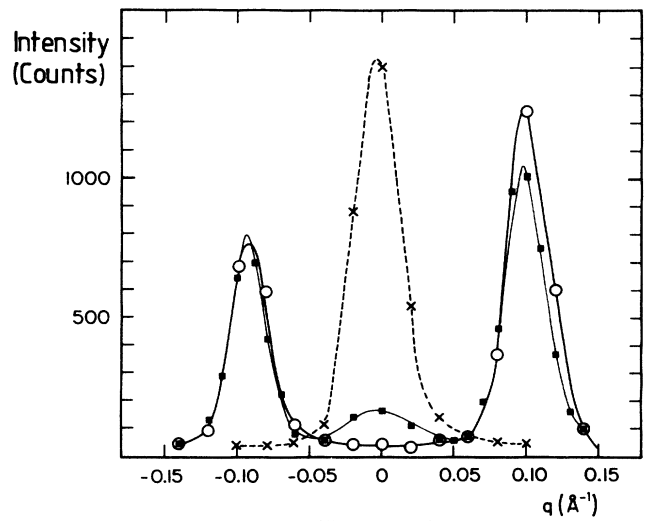

FIG. 12. Intensities of satellite reflections vs wave vector q. The scattering vector is $(-0.333a^*/13b^*+q/0)$. ×: 115 K (ϵ phase); ■: 114.1 K (ζ phase); ○: 112.7 K (ζ phase).

VII. DISCUSSION AND PHENOMENOLOGICAL DESCRIPTION

All experimental findings give strong evidence that δ-ϵ-ζ is a result of partial freezing out of the librational movements of the PA chains. A pure soft-mode behavior can be ruled out. In case of the incommensurate γ phase of the same compound, a plausible picture of the driving mechanism was obtained by taking into account molecular forces between the PA chains.[15] The incommensurate modulation was described as a result of a balance between next-neighbor interactions between neighbors of the same layer and of adjacent layers. In case of the δ-ϵ-ζ phase sequence a microscopic description seems to be much more complicated, because there are more degrees of freedom involved (lower symmetry of the problem). The aim of this section is to give a phenomenological description consistent with experimental results. Such a description has to include following facts: (1) wave-vector switching at the lock-in transition; (2) coincidence of the lock-in transition with freezing out of molecular dynamics; (3) frequency splitting of Cl(2) NQR line proportional to the square of the order-parameter η; (4) anisotropy energy term of third order in η, which appears in the ϵ phase.

The important question obviously concerns the *ground state* (ordered state) of the molecules, and how this state is established. It is known from the literature[10,11,12,28] that the $(C_nH_{2n+1}NH_3)_2MCl_4$ compounds with $n\geq 2$ have a common coupling scheme of the hydrogen bonds between the NH_3 groups and the MCl_4 layers: one bond to a Cl ion in an in-plane position [Cl(1)] and two bonds to Cl ions in an out-of-plane position [Cl(2)]. On the other hand, there are exactly two hydrogen bridges to each Cl(2) and one bridge to each Cl(1).[10] In addition, the ordered state must be consistent with the partially ordered state of the orthorhombic high-temperature phase (β and δ phase for PAMC). These conditions define a single possible solution for the hydrogen bonding pattern of all chains attached to the same layer (see Fig. 13). The hydrogen bonds for the NH_3 head determine the direction of the N—C bond and therefore the direction of the whole chain as long as the latter is rigid, which is the case for the propylammonium molecule. Molecular interactions and sterical restrictions between the CH_3 end groups of neighboring layers cause a correlation (interaction) between the hydrogen bond patterns of neighboring layers.

The part of the polarization vector which describes this ordering for the molecule tilt angles is $R_z \mid A1\rangle$ and $R_y \mid A3\rangle$. A Γ-point polarization vector (symmetry Γ_3^+) leads to the space group $C112_1/a$ ($Z=2$). It is also possible that the periodicity along $\mathbf{t}_1$ and $\mathbf{t}_2$ is doubled, i.e., the transition occurs at the Y point and yields a space group $Pbca$ ($z=4$).[29] The two solutions correspond to an in-phase and an antiphase tilting of adjacent layers.[29] The above considerations do not take into account, however, a possible hindering between molecules, preventing a homogeneous tilt of the chains that would be consistent with the tilt of their NH_3 end groups.

It is known that incommensurate phases may occur as

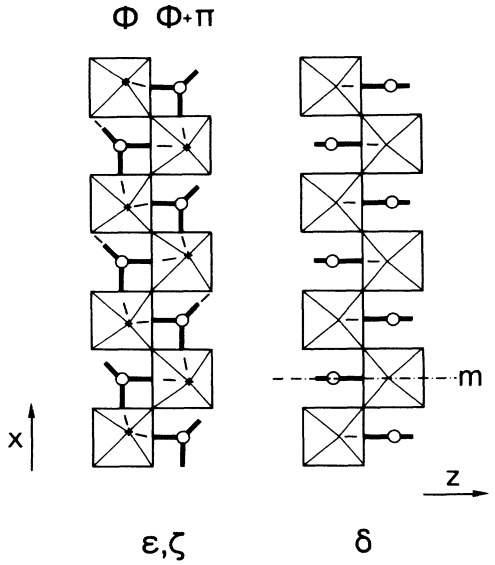

FIG. 13. Schematic structure of the layer planes in δ PAMC and ζ PAMC (ϵ PAMC). The modulation phase angle Φ of neighboring rows differs by π.

a consequence of competition between nearest-neighbor and next-nearest-neighbor interactions, the two coupling constants being of different sign.[30] In our case the nearest-neighbor interaction is given by the hydrogen bonds terminating at the same Cl ion. The next-nearest-neighbor interaction may result from molecular interactions between the layer planes, similar to the ones responsible for the incommensurate of γ PAMC.[15] As known from *D*-NMR (Sec. IV) the tilt around the *z* axis (tilt angle γ) is the largest component of the polarization vector of the incommensurate modulation. The molecules are rotated out of the mirror plane m_x of δ PAMC. As a consequence, the occupation probabilities n_1 and n_2 for the molecule being on the right-hand and left-hand sides of the mirror plane m_x become different. It is reasonable to assume that $|n_1-n_2|$ increases as a linear function of γ, and thus of the order parameter $|\eta|$. Now, the hydrogen bond interaction comes into play, which correlates n_1-n_2 along **a** irrespective of the modulation phase angle ϕ. This gives rise to a distortion of the sinusoidal modulation. What is especially unfavorable are phase differences of 180° between two domains. The chlorine NQR lines (see Sec. III) indeed show that only the domains $\phi\approx 0°$, $+120°$, $-120°$ occur. Domains with $\phi\approx +60°$, $-60°$, 180° are not observed.

A description of the phase sequence in the framework of a Landau theory including a Lifshitz invariant[21] is obtained if a mode softening at the *S* point $\mathbf{k}=\mathbf{g}_1/2$ or $\mathbf{g}_2/2$ (see Fig. 14) is assumed. At this point all modes are doubly degenerate and have the same symmetry (the irreducible representations ζ_1 and ζ_2 of Table III become equivalent at the *S* point). The order parameter has four components: Q_1, Q_1^*, Q_2, Q_2^*. Because of the existence of the Lifshitz invariants

$$L_x=\left[Q_1\frac{dQ_1^*}{dx}-Q_1^*\frac{dQ_1}{dx}\right]-\left[Q_2\frac{dQ_2^*}{dx}-Q_2^*\frac{dQ_2}{dx}\right],$$

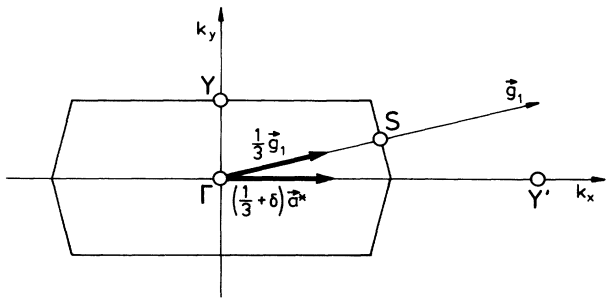

FIG. 14. The modulation wave vectors $(1/3+\delta)\mathbf{a}^*$ of ϵ PAMC and $\mathbf{g}_1/3$ of ζ PAMC in the first Brillouin zone.

$$L_y=\left[Q_1\frac{dQ_1^*}{dy}-Q_1^*\frac{dQ_1}{dy}\right]+\left[Q_2\frac{dQ_2^*}{dy}-Q_2^*\frac{dQ_2}{dy}\right],$$

the modulation does not freeze out with $\mathbf{k}=\mathbf{g}_1/2$, but with an incommensurate **k** vector $\mathbf{k}_0$ near $\mathbf{g}_1/2$ somewhere in the (k_x,k_y) plane. Neglecting any anisotropy in the density of free energy, $\mathbf{k}_0$ would have two incommensurate components. There are, however, always Umklapp terms that introduce some anisotropy and reduce the number of phasen modes.[30] In our case one has to consider not only the lowest order Umklapp terms for $\mathbf{k}_0$ near $\mathbf{a}^*/3$, and $\mathbf{k}_c=\mathbf{g}_1/3$, but also for those Umklapp terms that couple order parameter and molecular tilt fluctuations. For this purpose an order parameter p_1 for the in-phase tilting (Γ point) and an order parameter p_2 for the antiphase tilting (*Y* point) is introduced. For a single plane both are defined as $p_{1,2}=n_1-n_2$. The relevant Umklapp terms at $\mathbf{g}_1/3$ are

$$\begin{aligned}U_3&=\tfrac{1}{2}u_3(Q_1^3+Q_1^{*3}+Q_2^3+Q_2^{*3}),\\ U_{p_1}&=\tfrac{1}{2}w_1(Q_1^3-Q_2^3+Q_1^{*3}-Q_2^{*3})\cdot p_1 .\end{aligned}\tag{10}$$

The components of the order parameter can be written as

$$Q_1=r\cos\psi\, e^{i\phi_1},\quad Q_2=r\sin\psi\, e^{i\phi_2}$$

and we get for a single domain of the ζ phase ($\psi=0$)

$$\begin{aligned}U_3&=u_3r^3\cos 3\phi_1 ,\\ U_{p_1}&=w_1p_1r^3\cos 3\phi_1 .\end{aligned}\tag{11}$$

Since the ζ phase is commensurate one, ϕ_1 is fixed and according to the symmetry of the phase $\phi_1=n(2\pi/3)$.

For the ϵ phase we introduce the order parameter η as $\eta=1/\sqrt{2}(Q_1-Q_2^*)$. The phase relations of Q_1 and Q_2 must be such that $L_y=0$ and the correct symmetry of the ϵ phase is obtained. This is the case for $\psi=\pi/4$, $\phi_2=\pi-\phi_1$, and $\eta=re^{i\phi_1}$.

The lowest-order Umklapp term in function of η only is

$$U_6'=\tfrac{1}{2}u_6(\eta^6+\eta^{*6})=u_6r^6\cos(6\phi_1) .$$

A coupling to p_2 is provided by a fourth-order term

$$U_{p_2}=\tfrac{1}{2}w_2p_2(\eta^3+\eta^{*3})=w_2p_2r^3\cos(3\phi_1) .\tag{12}$$

The existence of the terms U_{p_1} and U_{p_2} makes it evident that the lock-in transition is caused by a switching from p_2 to p_1, i.e., a reorientation of the hydrogen bonding pattern in every second layer. The ground state of the pattern is the in-phase solution (p_1). In an intermediate temperature range the antiphase tilting is favored.

Such a behavior is consistent with Raman experiments.[26] Whereas the freezing out of p_1 (Γ-point excitation) is well observed, the zone-boundary excitation p_2 is inaccessible for this technique. The second moment measurements of the proton line shapes (Sec. V) show that there are still a lot of dynamics present in ϵ-PAMC. p_2 probably does not adopt a large static value, but still fluctuates at low frequencies.

The contribution of p_2 to the efg tensors at the chlorine and deuterium sites can have two parts. First of all a charge redistribution takes place. It is also conceivable that the tilt angle γ contains a homogeneous part proportional to p_2, which would affect the D-NMR rotation patterns. The latter is, however, not observed. Above 125 K the rotation patterns are well described by a sinusoidally modulated tilt angle γ.

The hydrogen bonding coupling scheme is expected to give a large contribution to the efg tensor of the Cl(2) site (off-plane position). Defining ν_{20} as the frequency for $\eta=0$ and $p_2=0$ ($\langle p_2^2\rangle=0$) the NQR frequency for Cl(2) nuclei ν_2 may be written as

$$\nu_2=\nu_{20}+A\,|\eta|\cos\phi(x)+Bp_2^2 +C\,|\eta|\,p_2\cos[\phi(x)+\phi_0]\ . \tag{13}$$

The term Bp_2^2 accounts for the large deviation of the "center of mass" of the Cl(2) NQR lines from the extrapolated temperature dependence as obtained from the δ phase. The splitting between the two edge singularities contains a contribution proportional to $|\eta|p_2$. This term dominates, because the measured critical exponent of the splitting is nearly 2β (Fig. 4). It also means that p_2 becomes critical at T_I also. The order parameter postulated in Sec. III is thus identified as p_2.

The efg tensor at the Cl(1) site is much less affected by p_2 and is more sensitive to deformations of the layer planes. The line splitting is therefore proportional to $|\eta|$ in good approximation. The cubic U term revealed by Cl(1) NQR is obviously identical to U_{p_2} [Eq. (12)].

In Sec. VI the temperature behavior of the incommensurate part δ of the modulation wave vector was obtained in first approximation as $\delta(T)=\delta_0(1-\alpha\,|\eta|^2)$, where α is proportional to the square of the coefficient of the third-order invariant, in our case to $w_2^2p_2^2$. Hence, this temperature behavior may also explained by a large value of $\langle p^2\rangle$, whereas p_2 may vary in space and time. On the other hand, microscopic considerations and the observed phase difference of solitons imply that *locally* p_2 does not vanish. Considering the problem in k space, the fourth-order Umklapp term Up_2 becomes

$$U_{p_2}=\tfrac{1}{2}w_2(p_k\eta_k^3+p_K^*\eta_k^{*3})\delta(\mathbf{K}+3\mathbf{k}-2\mathbf{a}^*)\ ,$$

where $\mathbf{K}$ is near $\mathbf{a}^*$ (wave vector of p_2) and $\mathbf{k}=(\frac{1}{3}+\delta)\mathbf{a}^*$. It follows that $\mathbf{K}=(1-3\delta)a^*$. p_K is the leading Fourier component of p_2. The modulation wave length of p_2 is about $8a$ at T_I. So after every fourth lattice constant p_2 flips from one to the other possible orientation, related to each other by the lost mirror plane m_x (see Fig. 13). Such a modulation costs energy. If one assumes an increase proportional to $(3\delta)^2\,|p_K|^2$, U_{p_2} may be written as an effective fourth-order term in $|\eta|$ as

$$U_{p_2}=\tfrac{1}{2}(-\tilde{w}_0+\tilde{w}_1(3\delta)^2)\,|\eta_k|^4\ .$$

Together with the harmonic term

$$\tfrac{1}{2}[a_0(T-T_I)+a_1(\delta-\delta_0)^2]\,|\eta_k|^2\ ,$$

one arrives at the same temperature dependence of $\delta(T)$ as derived in the Appendix, namely,

$$\delta(T)=\delta_0\left[1-3\frac{\tilde{w}_1}{a_1}\,|\eta_k|^2\right]\ .$$

One expects that the isostructural compound $(C_3H_7NH_3)CdCl_4$ (PACC) exhibits a similar phase sequence as PAMC. Indeed it was recently found[33] that PACC undergoes a commensurate-incommensurate phase transition at 182 K. The lock-in transition occurs at the Y point to the space group $Pbca$ ($z=4$), which is the same as resulting from a condensation of p_2-type fluctuations (as discussed above).

There are two astonishing properties of this sequence. First, from the symmetry point of view, a direct second-order transition from $Cmca$ to $Pbca$ at the Y point is possible. Second, there is a large change of the modulation wavelength at the lock-in transition from $\mathbf{k}=0.42\mathbf{a}^*$ to $1.00\mathbf{a}^*$, where the first value is not too much different from the $0.37\mathbf{a}^*$ as measured in PAMC. This behavior supports our phenomenological theory postulating a softening at the S point and a lock-in transition driven by the freezing out of the orientational disorder of the N—C bonds, connected with a certain hydrogen bond pattern. The difference of the lock-in phases is due to different correlations of these bond directions between neighboring layers mediated via molecular interactions through the chains. In PAMC this correlation changes sign, in PACC it does not, thus having the antiphase correlation between neighboring layers in the incommensurate as well as the lock-in phase. The different behavior of PACC must originate from the somewhat larger cavities between the chlorine octahedra.

VIII. CONCLUSION

We have shown that the peculiarities of the δ-ϵ-ζ sequence find an explanation if the orientational disorder of the chains is taken into account. The switching of the modulation wave vector at the lock-in transition is due to a transition between two possible ground states of the NH_3 configuration. The antiphase correlation between neighboring layers present in the ϵ-phase changes to an in-phase correlation in the δ phase. The frozen-out NH_3 configurations of the two ground states are determined by next-neighbor interactions of hydrogen bonds and keep

the periodicity of the δ phase within the layers. This leads to an additional symmetry breaking of the ϵ phase. As a result a third-order lock-in term occurs instead of a sixth-order term which manifests in the temperature behavior of the chlorine NQR lines and of the incommensurate part of the modulation wave vector.

We have measured the critical exponent β of the order parameter of the ϵ phase by means of pure chlorine NQR, deuteron NMR, and neutron scattering. The average value is $\beta=0.38\pm0.02$. This value is in the range of the usually measured critical exponents β of one-dimensionally modulated systems with a two-component order parameter. These values are explained by the applicability of the XY model ($\beta=0.35$).[32]

It would be desirable to confirm the obtained results by a structural analysis of ϵ-PAMC with the help of x-ray scattering or neutron scattering. A direct proof of a phonon softening at the S point could be obtained by means of inelastic neutron at a full deuterated crystal.

ACKNOWLEDGMENTS

The authors wish to thank M. Loss for helpful discussions concerning the Appendix. This work was supported in part by the Swiss National Science Foundation.

APPENDIX

In this appendix a formula for the calculation of the incommensurate part $\delta(T)\mathbf{a}^*$ of the incommensurate modulation is derived. It is assumed that the amplitude r of the order parameter $\eta=re^{i\Phi(x)}$ does not depend on x. The Φ-dependent part of the density of free energy is written as

$$g_\phi=-i\kappa\left[\eta\frac{d\eta^*}{dx}-\eta^*\frac{d\eta}{dx}\right]+\tfrac{1}{2}\lambda\frac{d\eta}{dx}\frac{d\eta^*}{dx}+\tfrac{1}{2}\gamma(\eta^n+\eta^{n*})$$
$$=\left[-\kappa\frac{d\phi}{dx}+\tfrac{1}{2}\lambda\left[\frac{d\phi}{dx}\right]^2\right]r^2+\gamma r^n\cos n\phi\ .$$

Φ contains only the incommensurate part and is therefore slowly varying, which justifies the use of a continuum model. In the plane-wave case, which is exact for $r=0$, one finds $\Phi(x)=\delta_0 x$ with $\delta_0=\kappa/\lambda$. In general, δ is defined as the space average of $d\phi/dx$ between the boundaries of the crystal at $x=\pm L$.

$$\delta=\frac{1}{2L}\int_{-L}^{+L}\frac{d\phi}{dx}dx=\frac{\phi(L)-\phi(-L)}{2L}\ .$$

The Euler equation of g_Φ becomes, after one integration,

$$\frac{d\phi}{dx}=\left[\frac{2\gamma}{\lambda}r^{n-2}\cos(n\phi)+c^2\right]^{1/2},$$

where c^2 is the integration constant. With this equation the space average can be converted into a phase average over a period of Φ. We write

$$\frac{1}{\delta}=\frac{1}{\phi(L)-\phi(-L)}\int_{\phi(-L)}^{\phi(L)}\left[\frac{2\gamma}{\lambda}r^{n-2}\cos(n\phi)+c^2\right]^{-1/2}d\phi\ ,$$

which becomes for large L

$$\frac{1}{\delta}=\frac{n}{\pi}\int_0^{\pi/n}\left[\frac{2\gamma}{\lambda}r^{n-2}\cos(n\phi)+c^2\right]^{-1/2}$$
$$\equiv\frac{1}{c}F(c,r)\ .$$

The space average of $(d\phi/dx)^2$ is obtained in a similar way as

$$\frac{1}{2L}\int_{-L}^{L}\left[\frac{d\phi}{dx}\right]^2dx=c^2\frac{H(c,r)}{F(c,r)}\ ,$$

where

$$H(c,r)\equiv\frac{n}{\pi}\int_0^{\pi/n}\left[\frac{2\gamma}{\lambda}r^{n-2}\cos(n\phi)+c^2\right]^{1/2}d\phi\ .$$

The average of g_Φ is obtained as

$$\frac{1}{2L}\int_{-L}^{L}g_\phi\,d\phi=\left[-\frac{\kappa c}{F(c,r)}+\lambda c^2\frac{H(c,r)}{F(c,r)}-\tfrac{1}{2}\lambda c^2\right]r^2\ .$$

Minimization with respect to c yields the condition

$$cH(c,r)=\kappa/\lambda\ .$$

(Note that $\partial/\partial c[cH(c,r)]=cF(c,r)$). For small r

$$H(c,r)=1-\frac{1}{4}\frac{\gamma^2r^{2n-4}}{\lambda^2c^4}$$

and

$$F(c,r)=1+\frac{3}{4}\frac{\gamma^2r^{2n-4}}{\lambda^2c^4}\ .$$

As δ_0 is equal to c ($r=0$) one can write in first approximation

$$c=\frac{\kappa}{\lambda H(\delta_0,r)}\ \text{and}\ \delta=\frac{c}{F(\delta_0,r)}$$

and arrive at

$$\delta(T)=\delta_0\left[1-\frac{1}{2}\frac{\gamma^2}{\lambda^2\delta_0^4}r^{2n-4}\right].$$

*Present address: Institut für Atom- und Festkörperphysik, Freie Universität Berlin, Arnimallee 14, D-1000 Berlin 33, West Germany.

[1]P. Muralt, R. Kind, R. Blinc, and B. Zeks, Phys. Rev. Lett. **49**, 1019 (1982).

[2]W. Depmeier, Solid State Commun. **45**, 1089 (1983).

[3]W. Depmeier and S. A. Mason, Solid State Commun. **46**, 409 (1983).

[4]H. Cailleau, F. Moussa, and J. Mons, Solid State Commun. **31**, 521 (1979).

[5]E. R. Peterson and R. D. Willett, J. Chem. Phys. **56**, 1879 (1972).

[6]W. Depmeier, J. Solid State Chem. **29**, 15 (1979).

[7]W. Depmeier, J. Felsche, and G. Wildermut, J. Solid State Chem. **21**, 57 (1977).

[8]W. Depmeier and S. A. Mason, Solid State Commun. **44**, 719 (1982).

[9]I. H. Brunskill and W. Depmeier, Acta Crystallogr. A **38**, 132 (1982).

[10]G. Chapuis, Phys. Status Solidi A **43**, 293 (1977); Acta Crystallogr. B **34**, 1506 (1978).

[11]G. Chapuis, H. Arend, and R. Kind, Phys. Status Solidi A **31**, 449 (1975); **36**, 285 (1976).

[12]R. Blinc, B. Zeks, and R. Kind, Phys. Rev. B **17**, 3409 (1978); R. Kind, Ferroelectrics **24**, 81 (1981), and references cited therein.

[13]R. Kind, S. Plesko, P. Günter, J. Roos, and J. Fousek, Phys. Rev. B **24**, 4910 (1981).

[14]P. Muralt, P. Caravatti, R. Kind, and J. Roos, J. Phys. **19**, 1705 (1986).

[15]P. Muralt, J. Phys. C **19**, 1689 (1986).

[16]See, for instance, M. Izumi, J. D. Axe, G. Shirane, and K. Shimaoka, Phys. Rev. B **15**, 4392 (1976); A. D. Bruce and R. A. Cowley, J. Phys. C **11**, 3609 (1978).

[17]A. Janner and T. Janssen, Phys. Rev. B **15**, 643 (1977); P. M. De Wolf, T. Janssen, and A. Janner, Acta Crystallogr. A **37**, 625 (1981).

[18]W. Depmeier and S. A. Mason, Acta Crystallogr. B **34**, 920 (1978).

[19]O. V. Kovalev, *Irreducible Representations of the Space Groups* (Gordon and Breach, New York, 1965).

[20]R. Geick and K. Strobel, J. Phys. C **10**, 4221 (1977).

[21]L. D. Landau and E. M. Lifshitz, *Statistical Physics* (Pergamon, London, 1958).

[22]M. Sutton and R. L. Armstrong, J. Magn. Res. **47**, 68 (1982).

[23]See, e.g., S. Plesko, R. Kind, and H. Arend, Phys. Status Solidi A **61**, 87 (1980).

[24]See, e.g., R. Blinc, Phys. Rep. **79**, 331 (1981).

[25]See, e.g., A. A. Maradudin and S. A. Vosko, Rev. Mod. Phys. **40**, 1 (1968).

[26]R. Mokhlisse, Ph.D. thesis, Université de Bordeaux I, 1983 (unpublished).

[27]See, e.g., J. D. Axe, M. Izumi, and G. Shirane, *Modern Problems in Condensed Matter Sciences* (North-Holland, Amsterdam, 1986), Vol. 14.2.

[28]D. E. Moncton, I. D. Axe, and F. I. DiSalvo, Phys. Rev. B **16**, 801 (1977).

[29]R. Kind, Phys. Status Solidi A **44**, 661 (1977).

[30]T. Janssen and J. A. Tjon, Phys. Rev. B **25**, 3767 (1982).

[31]T. I. Schäfer and W. Kleemann, Ferroelectrics **55**, 163 (1984).

[32]R. A. Cowley and A. D. Bruce, J. Phys. C **11**, 3577 (1978).

[33]G. Chapuis and B. Doudin, 9th European Crystallographic Meeting, Torino, Italy, 1985 (unpublished); R. Mokhlisse, M. Cousi, N. B. Chanh, Y. Haget, C. Hauw, and A. Meresse, J. Phys. Chem. Solids **46**, 187 (1985).